JCTC Journal of Chemical Theory and Computation
Article
pubs.acs.org/JCTC

SCC-DFTB Parametrization for Boron and Boranes

Bernhard Grundkötter-Stock,[†] Viktor Bezugly,[‡,§] Jens Kunstmann,[‡] Gianaurelio Cuniberti,[‡,§] Thomas Frauenheim,[†] and Thomas A. Niehaus*[,∥]

[†]Bremen Center for Computational Materials Science, Universität Bremen, Am Fallturm 1, 28359 Bremen, Germany
[‡]Institute for Materials Science and Max Bergmann Center of Biomaterials, Dresden University of Technology, 01062 Dresden, Germany
[§]Division of IT Convergence Engineering, POSTECH, Pohang 790-784, Republic of Korea
[∥]Department of Theoretical Physics, University of Regensburg, 93040 Regensburg, Germany

ABSTRACT: We present the results of our recent parametrization of the boron−boron and boron−hydrogen interactions for the self-consistent charge density-functional-based tight-binding (SCC-DFTB) method. To evaluate the performance, we compare SCC-DFTB to full density functional theory (DFT) and wave-function-based semiempirical methods (AM1 and MNDO). Since the advantages of SCC-DFTB emerge especially for large systems, we calculated molecular systems of boranes and pure boron nanostructures. Computed bond lengths, bond angles, and vibrational frequencies are close to DFT predictions. We find that the proposed parametrization provides a transferable and balanced description of both finite and periodic systems.

1. INTRODUCTION

Since the discovery of the element boron, the structural features of pure boron and boron hydrogen systems have been investigated intensely due to their distinction from the bonding situation found in organic compounds and related systems.[1−3] The diversity is attributed to the electron poorness of boron, meaning that the number of valence orbitals exceeds the number of valence electrons, giving rise to bonds formed by two electrons between three centers, so-called 2e3c bonds. One of the best known examples of this bonding scheme is found in diborane, B_2H_6, whose structure was subject to discussion for some time.[4] But also in other structures, uncommon bonding situations are found, so the whole series of boranes and borates are not properly described by Lewis structures but by concepts developed by Lipscomb, Wade, and Williams.[5−8]

In addition to these fascinating molecular systems, stable quasi-planar and tubular clusters of elemental boron were first predicted[9,10] and later observed experimentally.[11−13] On the basis of these findings, the existence of more complex pure boron nanostructures like boron fullerenes,[14,15] nanotubes, and two-dimensional sheets has been predicted.[16−21] These nanostructures are expected to have interesting properties for application in future nanoscaled devices. Recently, first successes in the synthesis and characterization of boron nanotubes[22−24] and the first hints on their real atomic structure and electronic properties[23,25] have been reported. Also, in its bulk phases, boron exhibits a remarkable complexity. All elemental bulk modifications are based on a three-dimensional framework of slightly distorted B_{12} icosahedra. The currently known elemental bulk phases are α-rhombohedral (α-B_{12}),[26,27] β-rhombohedral,[28] β-tetragonal,[29] and the γ-orthorhombic (γ-B_{28}) phases.[30−32] In all of these phases, boron is superhard and has semiconducting properties.

Given that the structural features of these systems are outstanding and the size of nanostructures favor computationally less demanding methods than *ab initio* schemes, we propose here a parametrization for the boron−boron and boron−hydrogen interactions in the SCC-DFTB method.[33−35] This approximate DFT scheme is shortly introduced in section 2, which also contains computational details and information on the protocol followed to generate the present parametrization. The results in section 3 cover both finite molecular systems and periodic nanostructures to illustrate the transferability of the approach. A detailed comparison with respect to DFT and semiempirical methods applicable to boron systems is then provided, which is summarized in section 4.

2. METHODS

2.1. Density Functional-Based Tight Binding (DFTB).

The SCC-DFTB method has already been the subject of several reviews[36,37] and will be described here only briefly. In order to derive the scheme, the total energy of DFT, which is a functional of the electron density $n(\vec{r})$, is expanded up to second order around a given reference density $n_0(\vec{r})$ with $n(\vec{r}) = n_0(\vec{r}) + \delta n(\vec{r})$:[35]

$$E_{\mathrm{tot}} = \sum_i^{\mathrm{occ}} \langle \Psi_i | \hat{H}[n_0] | \Psi_i \rangle - \frac{1}{2} \iint \frac{n_0(\vec{r})\, n_0(\vec{r}')}{|\vec{r} - \vec{r}'|} \, \mathrm{d}\vec{r}' \, \mathrm{d}\vec{r} + E_{\mathrm{xc}}[n_0] - \int V_{\mathrm{xc}}[n_0](\vec{r})\, n_0(\vec{r}) \, \mathrm{d}\vec{r} + E_{\mathrm{ii}} + \frac{1}{2} \iint \left[\frac{1}{|\vec{r} - \vec{r}'|} - \left. \frac{\delta^2 E_{\mathrm{xc}}}{\delta n(\vec{r})\, \delta n(\vec{r}')} \right|_{n_0} \right] \times \delta n(\vec{r})\, \delta n(\vec{r}') \, \mathrm{d}\vec{r} \, \mathrm{d}\vec{r}' \quad (1)$$

Here, $\hat{H}[n_0]$ is the usual Kohn−Sham Hamiltonian evaluated at the reference density. E_{xc} and V_{xc} denote the exchange-

Received: October 13, 2011
Published: February 1, 2012

correlation (xc) energy and potential, respectively, while the term E_{ii} stands for the ion−ion repulsion. The following further approximations are applied:

(1) The Kohn−Sham (KS) orbitals Ψ_i are represented in a minimal basis of pseudoatomic orbitals ϕ_μ ($\Psi_i = \sum_\mu c_{\mu i}\phi_\mu$), which are determined from an atomic DFT calculation with an additional harmonic potential $(r/r_c)^2$ for confinement with respect to the covalent radius r_0.[33] The confinement radii, r_c, for density and wave function are chosen separately. While the confinement radius for the density, r_{dc}, accounts for the compressed atomic densities found in (molecular) systems, the confinement radius for the wave function, r_{wfc}, equals more a basis set optimization also known for *ab initio* methods. Although r_{wfc} could also be chosen to be different for each type of atomic orbital, usually it is chosen to be the same for s and p functions. We use the gradient corrected Perdew−Burke−Ernzerhof (PBE)[44] exchange-correlation functional in this study. From the resulting Hamilton matrix elements, $H^0_{\mu\nu}$, only diagonal elements, $H^0_{\mu\mu}$, and two center, nondiagonal elements are kept. While for $H^0_{\mu\mu}$ the atomic eigenvalues are taken, the $H^0_{\mu\nu}$ are given by

$$H^0_{\mu\nu} = \langle\varphi_\mu|\hat{T} + \hat{V}_{\text{eff}}[n^0_A + n^0_B]|\varphi_\nu\rangle;\ \mu \in A,\ \nu \in B \tag{2}$$

where V_{eff} is the effective KS potential and n^0_A represents the densities of the neutral atoms A. These elements are tabulated together with the overlap matrix elements $S_{\mu\nu}$, with respect to the inter atomic distance $R_{AB} = |\vec{R}_A - \vec{R}_B|$.

(2) The density fluctuations δn are written as a superposition of atomic contributions δn_A, which are approximated by point charges Δq_A. To gain these, the charge difference between the atom in the molecule (q_A) and its neutral form (q^0_A) are calculated by Mulliken analysis:

$$\delta n = \sum_A \delta n_A \approx \sum_A \Delta q_A = \sum_A (q_A - q^0_A) \tag{3}$$

$$q_A = \frac{1}{2}\sum_i^{\text{occ}} \sum_{\mu\in A} \sum_\nu (c_{\mu i}{}^* c_{\nu i} S_{\mu\nu} + c_{\nu i}{}^* c_{\mu i} S_{\nu\mu}) \tag{4}$$

The term involving the second derivative of the total energy is then further approximated by an interpolation function γ_{AB}, determined from analytical evaluation of the Coulomb interaction of two spherical charge distributions located at the atomic positions $\vec{R}_A$ and $\vec{R}_B$. For the case A = B, it represents the chemical hardness of atom A.

(3) The remaining terms of eq 1, which only depend on the reference density n_0, are collected in a single energy contribution E_{rep}. This E_{rep} is approximated by a sum of short-range repulsive potentials, which depend on the diatomic distance R_{AB} only:

$$\begin{aligned} E_{\text{rep}} &= E_{ii} - \frac{1}{2}\iint \frac{n_0(\vec{r})\, n_0(\vec{r}')}{|\vec{r} - \vec{r}'|}\, d\vec{r}\, d\vec{r}' \\ &\quad + E_{xc}[n_0] - \int V_{xc}[n_0](\vec{r})\, n_0(\vec{r})\, d\vec{r} \\ &\approx \sum_{AB} U_{AB}(R_{AB}) \end{aligned}$$

Hence, the SCC-DFTB total energy reads

$$E_{\text{tot}} = \sum_i^{\text{occ}} \sum_{\mu\nu} c^i_\mu c^i_\nu H^0_{\mu\nu} + \frac{1}{2}\sum_{AB} \gamma_{AB}\Delta q_A \Delta q_B + E_{\text{rep}} \tag{5}$$

Application of the variational principle with respect to the MO coefficients $c_{\mu i}$ leads to the corresponding Kohn−Sham equations:

$$\sum_\nu c_{\nu i}(H_{\mu\nu} - \varepsilon_i S_{\mu\nu}) = 0 \tag{6}$$

$$H_{\mu\nu} = H^0_{\mu\nu} + \frac{1}{2}S_{\mu\nu}\sum_C (\gamma_{AC} + \gamma_{BC})\Delta q_C;\ \mu \in A,\ \nu \in B \tag{7}$$

These must be solved iteratively, because the Hamilton matrix elements depend on the Mulliken charges, which in turn depend on MO coefficients $c_{\mu i}$. This characterizes the self-consistent charge DFTB (SCC-DFTB) method.

The repulsive pair potentials, $U_{AB}(R_{AB})$, are constructed by performing DFT calculations for a reference system at various interatomic distances R_{AB} and subtracting from the DFT total energy the first two terms of eq 5, evaluated at the same geometry. Interpolation of the data points by means of polynomials or spline functions provides a continuous potential for the target element pair.

Therefore, to parametrize an element for the SCC-DFTB method, the following steps have to be taken:

1. Perform DFT calculations on the neutral atom to determine the LCAO basis functions ϕ_μ and the reference density n^0_A.
2. Determine suitable confinement radii for the density (r_{dc}) and wave function (r_{wfc}).
3. Numerically integrate Hamiltonian ($H_{\mu\nu}$) and overlap ($S_{\mu\nu}$) matrix elements, and tabulate the values as a function of the interatomic distance.
4. Obtain E_{rep} as stated above for every element combination under interest using suitable reference systems.

The transferability of the parameters has to be subject to further testing.

2.2. Choice of Basis Set and Confinement Radii.

Intending to extend the well established *mio* set[35,38,39] of Slater−Koster (SK) files for selected first and second row elements (the *mio* set includes the pair potentials for the elements H, C, N, O, and S), we used, in addition to the new boron−boron and boron−hydrogen, the existing hydrogen−hydrogen interaction of that set. Although boron is known for unorthodox bonding situations and d orbitals might help as polarization functions in such, we found the restriction of using only up to p orbitals sufficient for our SCC-DFTB parametrization.

Previous parametrizations for other elements and their combinations correlated the used confinement radii with the covalent radius (for boron, r_0 = 82 pm) of the atom. It was found that 5 and approximately 2 times the covalent radius are reasonable confinement radii for the atomic density and wave function, respectively. Using these values as a starting point, confinement radii in the range of 3−10 and 1.5−3.5 times the covalent radius for the density and the wave function, respectively, were tested by geometry optimizations. These were performed for the whole (transferability) test set of molecular systems, which is described in detail later. For each combination of confinement

Table 1. Selected Atomic Distances in Molecular Systems (values in Å)[a]

molecule		B3LYP/6-31G(d)	PBE/6-31G(d)	AM1	MNDO	DFTB (MatSci)	DFTB (new)
B_2H_2	B−B	1.525	1.545	1.584	1.603	1.519	1.508
	H−B	1.176	1.171	1.199	1.160	1.204	1.185
B_2H_4	B−B	1.641	1.632	1.513	1.572	1.625	1.639
	H−B	1.201	1.212	1.190	1.159	1.214	1.201
B_2H_6	B−B	1.770	1.767	1.752	1.754	1.797	1.796
	H−B	1.191	1.201	1.192	1.164	1.211	1.197
	B−H−B	1.317	1.325	1.329	1.350	1.363	1.308
B_3H_5	B−B	1.638	1.626	1.509	1.567	1.622	1.642
	H−B	1.200	1.200	1.190	1.160	1.214	1.201
B_4H_6	B−B	1.639	1.633	1.513	1.571	1.623	1.645
	H−B	1.200	1.211	1.191	1.160	1.214	1.201
B_4H_{10}	B−B	1.724	1.721	1.660	1.752	1.663	1.696
	H−B	1.191	1.202	1.193	1.166	1.212	1.198
	B−H−B	1.257	1.272	1.268	1.257	1.337	1.266
	B−**H−B**	1.417	1.420	1.413	1.515	1.381	1.366
B_5H_9	B−B	1.695	1.700	1.668	1.759	1.721	1.718
	H−B	1.186	1.197	1.185	1.149	1.210	1.194
	B−H−B	1.348	1.357	1.348	1.292	1.373	1.321
B_{12}	B−B	1.643	1.643	1.659	1.657	1.645	1.669
$B_5H_5^{2-}$	B−B	1.676	1.686	1.518	1.592	1.665	1.679
	H−B	1.220	1.228	1.190	1.160	1.253	1.223
$B_6H_6^{2-}$	B−B	1.735	1.743	1.726	1.734	1.736	1.744
	H−B	1.223	1.232	1.187	1.158	1.244	1.227
$B_7H_7^{2-}$	B−B	1.829	1.831	1.783	1.836	1.869	1.831
	H−B	1.221	1.230	1.189	1.163	1.240	1.225
$B_8H_8^{2-}$	B−B	1.821	1.819	1.780	1.843	1.884	1.824
	H−B	1.217	1.225	1.190	1.166	1.237	1.221
$B_9H_9^{2-}$	B−B	1.712	1.719	1.580	1.846	1.726	1.725
	H−B	1.215	1.225	1.192	1.166	1.233	1.226
$B_{10}H_{10}^{2-}$	B−B	1.821	1.820	1.760	1.831	1.822	1.798
	H−B	1.211	1.221	1.189	1.166	1.231	1.222
$B_{11}H_{11}^{2-}$	B−B	2.026	2.011	1.910	2.061	2.029	1.956
	H−B	1.210	1.221	1.194	1.170	1.231	1.229
$B_{12}H_{12}^{2-}$	B−B	1.787	1.791	1.758	1.817	1.825	1.793
	H−B	1.208	1.217	1.188	1.166	1.227	1.217
RMS error in %			0.59	3.48	4.69	2.47	1.02

[a]The root mean square (RMS) error with respect to B3LYP is given for the full set in the last row. Bold printing indicates the respective part of a 2e3c bond.

radii, the repulsive potential had to be determined in order to accomplish the geometry optimizations. As the best confinement radii, we took the combination leading to the smallest deviations from DFT/B3LYP calculations with a 6-31G(d) basis set with respect to interatomic distances and angles. This procedure led to values of $4.65r_0$ and $3.23r_0$ for the density and wave function radii, respectively.

2.3. Determination of the Repulsive Potential. According to the parametrization protocol of the SK files already at hand, the DFT calculations for E_{rep} were performed, like they were for the *mio* set, using the exchange-correlation functional B3LYP and basis set 6-31G(d) with the program Gaussian 2003.[40] As reference systems, we chose B_2H_4 in D_{2d} symmetry, which is a stable configuration according to frequency calculations, for both pairwise interactions. For the H−B interaction, all four hydrogens were set to equal distances R_{AB}, conserving the symmetry of the system. Results were divided by 4, the number of extended distances, to get the interaction of one pair H−B. A known shortcoming of the *mio* set is its overbinding of roughly 10 kcal/mol per bond, which is clearly observable in atomization energies but does not surface in isodesmic reactions. In order to achieve a balanced description of reactions that conserve the number of shared electron pairs, we shifted the repulsive potentials for H−B and B−B to obtain a consistent overbinding.[41] At a certain cutoff distance r_{cut}, the repulsive potential is then smoothly brought to zero to ensure correct dissociation. For the present parametrization, the cutoff values were chosen to minimize the errors in bonding distances, angles, and vibrations, which lead to the values r_{cut}^{H-B} = 1.36 Å and r_{cut}^{B-B} = 1.99 Å. A large sensitivity on the cutoff values was found especially for compounds with 2e3c bonds like B_4H_{10}.

3. RESULTS AND DISCUSSION

3.1. Molecular Systems. *3.1.1 Geometries.* Our test set for the new parameters included structures of *closo-*, *nido-*, and *archano*-boranes with uncharged and charged systems. In order to evaluate whether the B−B interaction is described correctly, also molecules formally forming solely two electron bonds were added. These molecules could be referred to as "carbon-like" and are hypothetical. Examples of such molecules are B_3H_5 and B_4H_6.

dx.doi.org/10.1021/ct200722n | J. Chem. Theory Comput. 2012, 8, 1153−1163

Table 2. Selected Angles in Molecular Systems (Values in Degrees)[a]

molecule		B3LYP/6-31G(d)	PBE/6-31G(d)	AM1	MNDO	DFTB (MatSci)	DFTB (new)
B_2H_2	H−B−B	180.0	180.0	129.18	132.23	180.0	180.0
B_2H_4	H−B−B	122.3	122.3	120.5	121.8	122.1	123.1
	H−B−H	115.4	114.8	118.9	116.4	115.8	113.7
B_2H_6	H−B−B	119.0	119.0	118.1	119.5	119.5	120.0
	B−H−B	84.4	83.7	82.5	81.0	82.5	86.7
	H−B−H	122.1	122.0	123.9	121.0	121.0	119.9
B_3H_5	B−B−B	129.4	130.8	129.5	127.5	122.2	129.1
	H−B−B	121.7	121.5	120.2	121.5	121.7	122.5
	H−B−H	116.4	116.4	119.5	117.0	116.6	115.0
B_4H_6	B−B−B	128.3	128.3	127.9	127.3	121.8	128.4
	H−B−B	114.9	114.4	115.9	116.2	118.3	114.9
	H−B−H	116.3	116.2	119.6	117.0	116.5	115.1
B_4H_{10}	B−B−B	98.6	98.1	102.0	103.7	97.3	99.2
	H−B−B	115.7	115.7	112.2	111.5	126.3	121.5
	B−H−B	88.1	86.5	86.3	84.8	95.2	92.3
	H−B−H	119.0	118.4	126.3	122.9	120.4	117.3
B_5H_9	B−B−B	64.1	63.8	66.1	64.9	65.8	64.5
	H−B−B	131.4	131.7	129.7	118.1	129.8	131.0
	B−H−B	83.7	82.9	85.0	86.4	85.8	87.9
	H−B−H	90.8	90.3	93.8	102.7	90.4	92.1
B_{12}	B−B−B	179.4	179.4	141.1	178.7	179.9	179.8
$B_5H_5^{2-}$	B−B−B	56.9	57.2	49.9	52.1	53.4	55.8
	H−B−B	129.2	128.7	140.7	137.9	133.5	130.4
$B_6H_6^{2-}$	B−B−B	60.0	60.0	60.1	60.1	60.0	60.0
	H−B−B	135.0	135.0	136.9	135.1	135.00	135.0
$B_7H_7^{2-}$	B−B−B	63.1	63.0	63.4	63.5	63.6	63.0
	H−B−B	140.4	140.7	139.5	139.8	139.3	140.7
$B_8H_8^{2-}$	B−B−B	60.2	60.1	60.4	59.8	61.0	60.6
	H−B−B	122.4	122.6	119.5	120.6	121.2	121.3
$B_9H_9^{2-}$	B−B−B	58.6	58.5	62.1	52.7	56.9	57.8
	H−B−B	127.2	127.2	131.0	130.9	127.2	127.0
$B_{10}H_{10}^{2-}$	B−B−B	90.0	90.0	89.9	90.0	90.0	90.0
	H−B−B	131.8	131.8	131.3	131.2	130.8	131.6
$B_{11}H_{11}^{2-}$	B−B−B	60.9	60.8	61.5	62.0	61.2	61.0
	H−B−B	107.2	106.3	108.0	110.2	109.6	105.4
$B_{12}H_{12}^{2-}$	B−B−B	60.0	60.0	59.9	59.8	60.0	60.0
	H−B−B	121.7	121.7	121.7	121.5	121.7	121.7
rms error in %			0.44	3.40	3.36	2.57	1.17

[a]The RMS error with respect to the B3LYP results is given in the last row.

For the test of transferability, we calculated interatomic distances and angles for a set of 16 molecules (B_2H_2, B_2H_4, B_2H_6, B_3H_5, B_4H_6, B_4H_{10}, B_5H_9, $B_{12}(D_{3h})$, $B_nH_n^{2-}$ with $n = 5-12$). The results were compared to DFT calculation with the hybrid functional B3LYP[42,43] and 6-31G(d) basis set as a reference, together with values for the gradient corrected PBE functional and the semiempirical wave-function-based methods AM1[45] and MNDO[46] as well as with the existing DFTB-MatSci parametrization.[47,48] Our findings for the distances are given in Table 1 and for the angles in Table 2.

We decided to use B3LYP calculations as a reference instead of experimental results in order to have a uniform reference. While B3LYP calculations could be performed for every structure, experimental data for the hypothetical "carbon-like" systems were not at hand since these have not been synthesized up to now. Moreover, experimental information on bond distances is often obtained by single crystal X-ray diffraction, which cannot be directly compared to the calculated gas phase structures under discussion.

The error for our SCC-DFTB of about 1% is comparable to PBE, while AM1 and MNDO show larger deviations (about 3 and 4%, respectively). For DFTB-MatSci, the average result is somewhere in between. All methods do quite well for small, uncharged molecules. Even for the hypothetical molecules, the semiempirical methods yield satisfactory results, although these are probably not part of their parametrization set. An exception for MNDO are the *archano* structure B_4H_{10} and the *nido* structure B_5H_9, where the 2e3c bonds are broken and therefore the molecules are deformed. In the case of B_5H_9, this deformation is so drastic that the *nido* character of the molecule is changed to an *archano*-like character, meaning that the basic structural polyhedron is changed. The errors of AM1 for B_{12} are fortified by buckling of the originally planar structure. The limitations of AM1 and MNDO are identifiable for the charged molecules, when compared to PBE and SCC-DFTB. DFTB-MatSci seems to be less exact for 2e3c bonds, where deviations of up to 8% were found, while the descriptions of terminal H−B bonds and B−B interactions are reasonable also for charged molecules. In the following, we focus

on the new parametrization and report SCC-DFTB results only for this SK set.

In $B_5H_5^{2-}$, $B_9H_9^{2-}$, and $B_{11}H_{11}^{2-}$, notable bond elongations of about 4% at most are observed for SCC-DFTB. Those are mainly leading to enlarging the closed cluster on one side and therefore clustering of atoms on the other. Still the symmetry of the molecules is conserved. While the clustering of atoms is observable for AM1 and MNDO, too, these methods also tend to break the symmetry, which lead to errors of up to 12% and 24%, respectively.

3.1.2. Vibrations. For five molecules out of the test set, a full normal-mode analysis was performed, yielding 108 vibrational frequencies in total. In Table 3, the SCC-DFTB results are compared to PBE/6-31G(d), AM1, and MNDO, while our reference is again B3LYP/6-31G(d), since experimental values are not available for all molecules and/or have an unresolved symmetry of the vibrational modes that might lead to assignment problems.

Table 3. RMS Error of Harmonic Vibrational Frequencies in % with Respect to the B3LYP/6-31G(d) Reference for Individual Molecules and the Full Test Set[a]

molecule	PBE/6-31G(d)	AMI	MNDO	DFTB
B_2H_4	6.47	13.68	16.78	8.36
B_2H_6	4.84	10.67	10.76	7.37
B_3H_5	6.36	17.01	19.15	8.98
B_4H_6	5.59	18.93	20.09	6.59
B_4H_{10}	4.60	9.99	10.33	4.57
full test set	5.57	14.05	15.42	7.17

[a]Prior to the normal mode analysis, the geometries of the molecules have been optimized at the respective level of theory.

In general, the agreement of SCC-DFTB and PBE with the reference is significantly better than those of AM1 and MNDO, as can be seen by the resulting RMS error. The performances for individual vibrational modes of B_2H_6 and B_4H_{10} are presented in Tables 4 and 5. The largest errors of SCC-DFTB occur for bending modes, while stretching modes are more accurately described. The mean of the absolute difference between DFT/B3LYP and SCC-DFTB is approximately 53 cm^{-1}. This is nearly the same as for PBE with 41 cm^{-1}, whereas the deviations for AM1 and MNDO are more than twice as big. The symmetry ordering of the modes is quite the same for B3LYP and PBE. AM1, MNDO, and SCC-DFTB have the same difficulties matching the ordering

Table 4. Harmonic Vibrational Frequencies of B_2H_6 in cm^{-1}[a]

symmetry	B3LYP/6-31G(d)	PBE/6-31G(d)	AM1	MNDO	DFTB
B_{2u}	356	305	320	402	357
A_g	797	792	787	819	749
A_u	852	832	871	853	747
B_{2g}	888	878	710	823	767
B_{1g}	947	917	966	972	813
B_{2u}	978	897	1128	1192	952
B_{1u}	1000	963	1169	1144	873
B_{3g}	1055	980	1228	1239	1055
B_{3u}	1205	1159	1113	1223	1083
A_g	1210	1161	1301	1308	1098
B_{3u}	1730	1688	1377	1530	1809
B_{2g}	1862	1851	1694	1815	1833
B_{1u}	2019	2020	2117	2303	2162
A_g	2203	2167	2252	2430	2230
B_{3u}	2638	2578	2814	2908	2650
A_g	2651	2590	2807	2905	2661
B_{1g}	2731	2670	2825	2972	2755
B_{2u}	2744	2683	2838	2981	2762

[a]Prior to the normal mode analysis, the geometries of the molecule have been optimized at the respective level of theory.

Table 5. Harmonic Vibrational Frequencies of B_4H_{10} in cm^{-1}[a]

symmetry	B3LYP/6-31G(d)	PBE/6-31G(d)	AM1	MNDO	DFTB
A_1	212	196	196	243	204
B_2	357	342	356	261	397
A_2	416	402	274	409	384
B_2	466	552	474	494	522
A_1	561	586	540	479	452
B_1	571	580	522	512	553
A_2	678	693	535	549	638
A_1	683	660	823	768	627
B_1	770	723	756	801	748
A_1	807	794	892	889	758
A_1	865	844	1036	1016	957
B_2	888	865	897	918	833
A_2	911	898	790	811	801
B_1	921	892	929	908	837
B_2	954	909	927	968	907
A_1	1021	965	1184	1187	1014
B_1	1027	986	1076	1084	929
A_2	1044	1002	1021	1017	930
A_2	1102	1059	1203	1212	1035
B_1	1120	1067	1211	1226	1081
B_2	1171	1125	1235	1249	1101
A_1	1187	1138	1242	1260	1110
B_2	1332	1309	1347	1400	1374
A_2	1462	1439	1410	1441	1461
B_1	1536	1493	1429	1460	1543
A_1	1579	1550	1546	1596	1582
A_1	2258	2187	2357	2489	2298
B_1	2260	2203	2373	2504	2282
B_2	2274	2212	2289	2476	2304
A_2	2284	2231	2291	2480	2296
B_2	2615	2545	2782	2871	2642
A_1	2620	2549	2781	2871	2646
A_1	2706	2638	2803	2916	2730
B_2	2708	2640	2829	2954	2740
B_1	2713	2659	2792	2912	2726
A_1	2722	2665	2831	2955	2743

[a]Prior to the normal mode analysis, the geometries of the molecule have been optimized at the respective level of theory.

3.1.3. Atomization Energies. A further stringent test for the accuracy of the new parametrization is given by atomization energies. As mentioned above, the repulsive potentials for H−B and B−B have been shifted to match the overbinding of the existing *mio* SK set. The required shift was determined for the B−B interaction on B_{12} and on BH_3 for the H−B interaction. In this way, the overbinding for each interaction could be isolated. Please note that the shifting process has usually only marginal influence on geometries and frequencies since the cutoff radius is chosen to be larger than any typical bonding distance. Tables 6 and 7 list the results of DFTB together with DFT results using B3LYP, PBE, and LDA exchange-correlation functionals. As usual, LDA strongly

Table 6. Atomization Energies in kcal/mol[a]

molecule	B3LYP/6-31G(d)	LDA/6-31G(d)	PBE/6-31G(d)	DFTB
B_{12}	1323.85	1662.03	1453.80	1563.95
BH_3	286.74	309.39	295.03	316.84
B_2H_2	266.20	302.65	337.10	300.43
B_2H_4	460.12	509.04	459.31	512.23
B_2H_6	622.64	685.83	614.26	732.58
B_3H_5	603.66	712.13	640.29	709.76
B_4H_6	812.05	914.12	820.47	906.67
B_4H_{10}	1107.73	1273.90	1128.64	1370.55
B_5H_9	1182.77	1377.93	1219.35	1464.34

[a]The spin polarization energy of isolated atoms was taken into account. No correction for zero point motion was performed.

Table 7. Overbinding Per Bond in kcal/mol with Respect to B3LYP/6-31G(d)[a]

molecule	LDA/6-31G(d)	PBE/6-31G(d)	DFTB
B_{12}	14.00	5.34	10.00
BH_3	7.42	2.64	10.03
B_2H_2	12.03	23.49	11.41
B_2H_4	9.66	−0.28	10.42
B_2H_6	6.93	−1.02	12.21
B_3H_5	15.37	5.12	15.16
B_4H_6	11.21	0.82	10.51
B_4H_{10}	8.66	1.03	13.83
B_5H_9	11.38	2.06	16.56
average	10.74	4.36	12.24

[a]The spin polarization energy of isolated atoms was taken into account. No correction for zero point motion was performed.

overbinds while the gradient corrected PBE and the hybrid functional B3LYP both give more accurate results. DFTB is found to yield similar results as LDA, and although the average overbinding of 12.24 kcal/mol per bond is close to the desired value of 10 kcal/mol, there are also values exceeding 16 kcal/mol. This overbinding for the molecule with the most B−H−B bonds in the test set (B_5H_9) suggests that 2e3c bonds are energetically not well enough described. However, the errors for B_2H_6 and B_4H_{10}, which also comprise B−H−B bonds to a large extent, are smaller than for B_3H_5, a carbon-like borane. Thus, a decisive clue why this is the case is missing.

3.1.4. Ionization Potentials. Another interesting topic, due to the molecules in our test set, is the (vertical) ionization potentials (IP) of the doubly charged *closo* clusters. Calculations on these systems have been performed by McKee et al.,[49] who found that in the series of covered clusters here, only $B_{12}H_{12}^{2-}$ should overcome the Coulomb repulsion and therefore has a positive, vertical ionization potential. The values of the IP are given in Table 8 and visualized in Figure 1. As one can see, we achieve the same trend of the IP as does DFT, although we get a slightly negative IP for $B12H_{12}^{2-}$. Any influence of spin polarization for DFTB[50] on the results has also been examined but was found to be of only marginal effect; therefore, those results are not shown. Given the fact that the DFTB basis set is roughly the same size as the STO-3G one, the proximity of the DFTB results to DFT with larger basis sets is remarkable.

3.2. Periodic Systems. To check the reliability of the DFTB parametrization for boron in periodic systems, we have performed geometry relaxation and electronic structure calculations of bulk elemental boron, three models of stable two-dimensional boron sheets, and three boron nanotubes obtained by rolling up

Table 8. Vertical Ionization Iotentials (eV) for Boron Hydride Dianions ($B_nH_n^{2-}$) Calculated at Different DFT Levels and with DFTB

n	McKee et al.[49]	LDA 6-311+ +G**	PBE 6-311+ +G**	B3LYP 6-311++G**	B3LYP STO-3G	DFTB
5	−2.60	−2.29	−2.12	−2.21	−6.27	−2.97
6	−1.50	−1.14	−0.78	−0.96	−4.29	−2.24
7	−1.00	−0.93	−0.58	−0.68	−3.68	−1.77
8	−1.69	−1.62	−1.73	−1.70	−4.57	−2.06
9	−1.20	−1.03	−1.22	−1.18	−3.98	−2.03
10	−0.27	−0.04	0.22	0.08	−2.28	−1.17
11	−0.54	−0.47	−0.54	−0.54	−2.88	−1.25
12	1.64	1.20	1.97	1.63	−0.03	−0.21

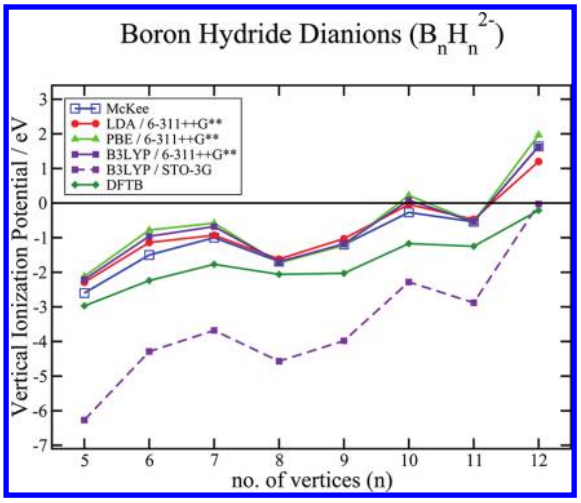

Figure 1. Plot of ionization potential (eV) for removing the first electron of the dianion ($B_nH_n^{2-} \rightarrow B_nH_n^{-}$). The structure of the ionized anion was not relaxed; i.e., vertical ionization potentials are computed. Reference data by McKee et al.[49] are also shown for comparison.

each of the three sheets. The DFTB calculations for periodic systems were also performed within the self-consistent charge (SCC) scheme. To speed up the convergence of the self-consistent loop during geometry relaxations, the molecular orbital occupations were determined according to a Fermi distribution function corresponding to an electronic temperature of 100 K. For the subsequent single point calculations at the converged geometries, the temperature was kept equal to zero. For each system, the energy was converged with respect to the number of *k* points.

In order to validate the DFTB results, for the same systems, full DFT calculations with the generalized gradient approximation[44] (called here DFT/PBE approach) were performed using the projector augmented wave method[51] as implemented in the VASP package.[52] The use of the PBE exchange-correlation functional as the reference here instead of the B3LYP is justified, as the former provides more reliable geometries and atomization energies of metallic and small-gap semiconducting systems than the latter.[53] Full geometry optimizations have been carried out, and the atomic forces were reduced to be below 1 meV/Å. For all of these calculations, the energy convergence over the number of *k* points was reached, and the tetrahedron method for *k*-integration was used.

3.2.1. Geometries. As a test system for bulk boron, the *α*-rhombohedral boron crystal[26,27] is chosen. Its rhombohedral unit cell comprises one B_{12} icosahedron. Figure 2 shows four

dx.doi.org/10.1021/ct200722n | J. Chem. Theory Comput. 2012, 8, 1153−1163

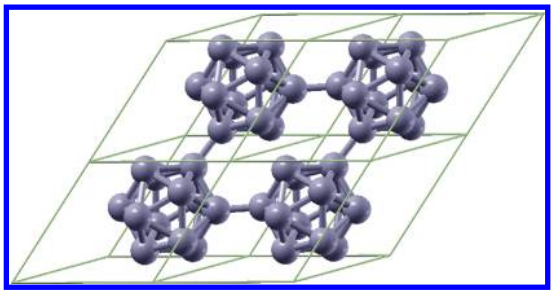

Figure 2. Schematic view of four neighboring unit cells of α-rhombohedral boron. One unit cell comprises a B_{12} icosahedron.

neighboring unit cells of α-rhombohedral boron. The three models of boron sheets studied here are the so-called α-sheet,[19] the buckled triangular sheet[17] (BT-sheet), and the distorted hexagonal sheet[18] (DH-sheet). The lattice structures of these sheets with the corresponding lattice vectors are shown in Figure 3.

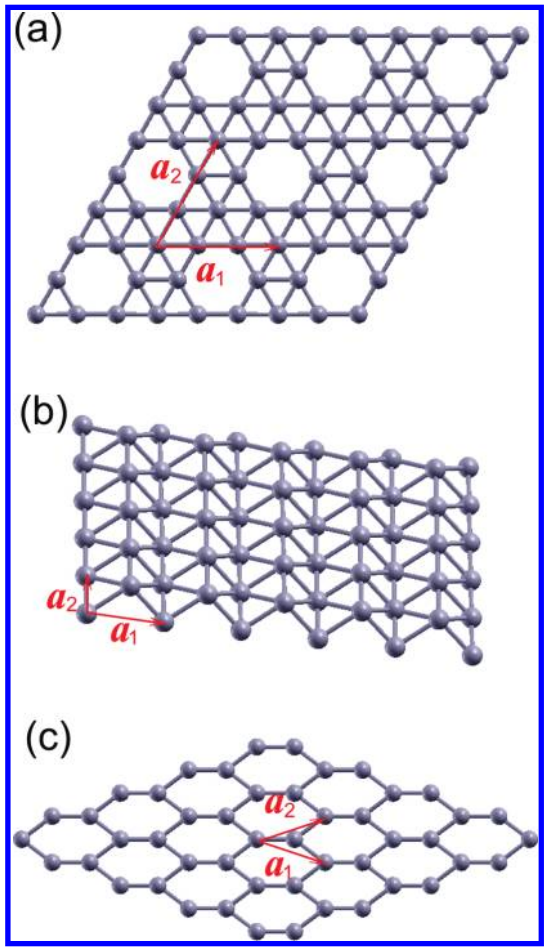

Figure 3. Schematic view of the three considered models of two-dimensional boron sheets: (a) α-sheet, (b) buckled triangular sheet, and (c) distorted hexagonal sheet; $\vec{a}_1$ and $\vec{a}_2$ are the lattice vectors.

Boron nanotubes (BNTs) are obtained by rolling up the corresponding boron sheet along the direction of the so-called chiral vector. The latter is expressed in terms of the sheet's lattice vectors as $\vec{C} = n\vec{a}_1 + m\vec{a}_2$. Knowing the lattice vectors of the original sheet, the structure of a particular nanotube is defined by the pair of numbers (n,m). Here, we present the calculations of a (4,0) α-BNT, a (0,12) BT-BNT, and a (4,4) DH-BNT, which originate from the α-sheet, the BT-sheet, and the DH-sheet, respectively (see Figure 4).

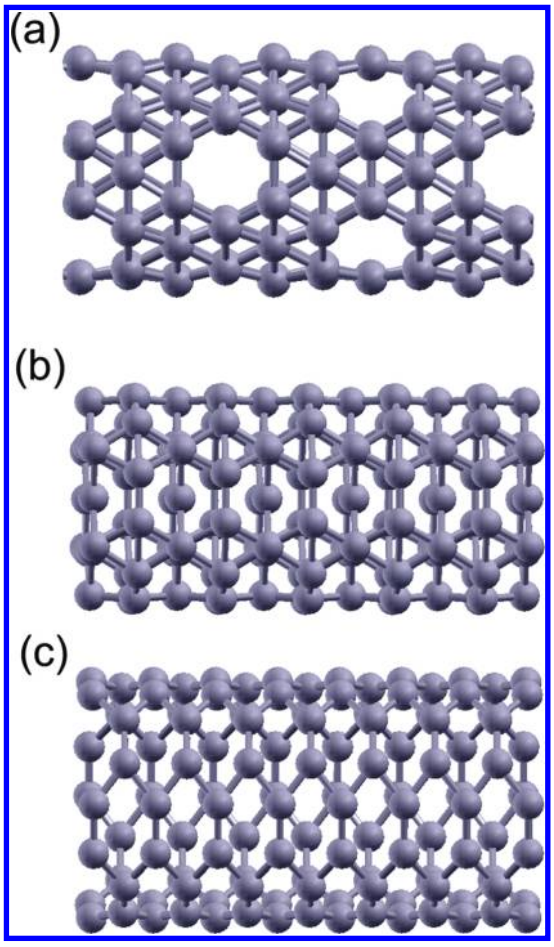

Figure 4. Schematic view of three boron nanotubes obtained by rolling up the three different boron sheets: (a) (4,0) α-BNT, (b) (0,12) BT-BNT, and (c) (4,4) DH-BNT.

Full geometry relaxation (optimization of lattice vectors and the atomic coordinates within a unit cell) was performed at both the DFTB and DFT/PBE levels of approximation. The results of geometry optimizations (bond lengths and angles) for each system are compared, and the root mean squares (RMS) of deviations in percent are summarized in Table 9.

Table 9. Overview of Deviation of the Geometric Parameters for Periodic Systems Calculations between DFT/PBE and DFTB (RMS in %)

system	bond lengths	angles
α-rhombohedral	1.7	1.0
α-sheet	5.0	1.9
BT-sheet	3.8	1.6
DH-sheet	1.3	1.4
α-BNT (4,0)	4.3	4.2
BT-BNT (0,12)	3.4	3.4
DH-BNT (4,4)	1.4	2.9

The overall agreement of the structures obtained with the two different methods is discernible. For several systems (bulk boron, DH-sheet, and the BNT derived from this sheet), the

dx.doi.org/10.1021/ct200722n | J. Chem. Theory Comput. 2012, 8, 1153–1163

average deviation of the geometric parameters is close to 2%. Other systems show larger deviations; however, they do not exceed 5%. Interestingly, comparing the RMS deviations of a boron sheet and the corresponding nanotube, one finds that average deviations of lengths are almost similar, while those of angles are roughly twice as high for the nanotubes than for the sheets. Compared to the results for molecular systems (see Table 1), the deviations of the geometric parameters in the case of periodic systems are larger. However, one has to emphasize here that the DFTB parametrization for boron was done in finite molecular systems using (i) a local basis set and (ii) the B3LYP exchange-correlation functional. Despite this, one can conclude that the standard geometry optimization procedures using new boron SK files is able to deliver reliable results not only for finite molecules but also for periodic structures.

3.2.2. Electronic Structures. In this section, we compare the band structures calculated with the DFTB and the DFT/PBE methods for each of the chosen periodic systems. To allow for an unbiased comparison, both types of electronic structure calculations are performed for a fixed geometry, namely, the relaxed DFT/PBE geometry. The results for the α-rhombohedral boron are presented in Figure 5. In general, the valence bands

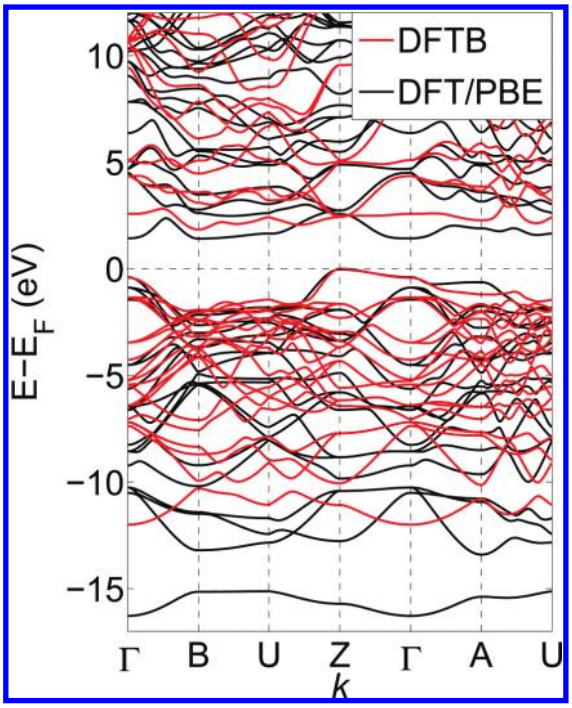

Figure 5. Comparison of band structures of α-rhombohedral boron obtained at the DFTB (red lines) and DFT/PBE (black lines) levels of approximation for the same geometry (taken from the DFT/PBE calculation).

qualitatively agree. For energies close to the Fermi level (E_F), the bands almost coincide; however, for energies far from E_F the two sets of bands deviate quite strongly: namely, the DFTB valence bands are shifted toward higher values with respect to the DFT/PBE bands. The deviation of conduction bands is also quite noticeable: the lowest DFTB conduction band lies higher compared to the corresponding DFT/PBE one.

Both calculation methods show that α-rhombohedral boron has an indirect band gap which is defined between the top of the valence band at the Z point and the bottom of the conduction band at the B point. The calculated band gap is equal to 1.840 eV for DFTB and 1.446 eV for DFT/PBE. The experimentally obtained values of the band gap for this system[54−56] range from 1.9 to 2.055 eV. Thus, both theoretical approaches underestimate the band gap of α-rhombohedral boron; however, the DFTB result is closer to the experimental value. The DFT/PBE values for the energy of the lowest conduction band at points B and Γ are almost equal to one another (1.446 and 1.460 eV, respectively). Earlier calculations[27] (with different exchange-correlation functional) gave similar results. However, the bottom of the conduction band (1.427 eV) was found to be at the Γ point, and the indirect band gap was defined between Z and Γ. In contrast, the DFTB value of the lowest conduction band at Γ is noticeably (by 0.736 eV) higher than at Z.

In the case of two-dimensional boron sheets (see Figure 6), the DFTB calculation reproduces the DFT band structures close to Fermi energy quite well (both valence and conduction bands). The deviations become larger for energies 2 eV and further away from E_F. However, the qualitative agreement for all valence bands is apparent, and the main difference between the two sets of bands is seen as a shift of DFTB valence bands upward. In the region of unoccupied states, the number of DFTB conduction bands is lower than that of DFT because of smaller DFTB basis set.

Similar conclusions as for boron sheets can be drawn for band structures of BNTs (in Figure 7, the bands are shown for the energy range from −3 to +3 eV). It is seen that even for such complicated structures like nanotubes with up to 64 atoms per unit cell (case of (4,0) α-BNT) the agreement between bands, obtained within DFTB and DFT/PBE approaches, is good.

The comparison of the electronic structures of different periodic systems shows that the DFTB parametrization is able to reproduce the band structures quite well for energies close to Fermi energy (up to 2 eV). Again, it has to be emphasized that the DFTB parametrization used here for the electronic structure calculation of periodic systems was constructed for finite molecules using a different basis set and exchange-correlation functional than those used in our benchmark periodic calculations. Therefore, these small deviations of the two sets of bands are to be expected. The energy bands start to noticeably deviate for energies far from E_F, which is seen as a "compression" of the DFTB set of the valence bands. This indicates that in our tight binding approach the so-called hopping integrals are underestimated. However, overall qualitative agreement of valence bands is obtained. Especially well reproduced are the bands of metallic systems (like boron sheets and tubes studied here), while the band structure near the band gap of nonmetallic systems cannot be accurately reproduced by DFTB. The problem here is a relatively small basis set for a proper calculation of unoccupied states, which results also in smaller number of DFTB conduction bands.

3.2.3. Cohesive Energies. In addition to energy bands, the cohesive (atomization) energies E^{coh} of periodic systems obtained with DFTB and DFT/PBE are compared for the optimized geometries. Cohesive energy is defined as $E^{coh} = E^{at} - E^{tot}/N$, where E^{at} and E^{tot} are the ground-state energies of a spin-polarized isolated boron atom and the whole system, respectively, and N is the number of atoms in the system. From this definition, it follows that positive values of E^{coh} correspond to bound (stable) structures. For periodic systems, E^{tot} is calculated for one unit cell, and N is equal to the number of atoms per unit cell. The cohesive energies of our test systems obtained with the two methods and the DFTB overbinding per bond are summarized in Table 10. The comparison shows that

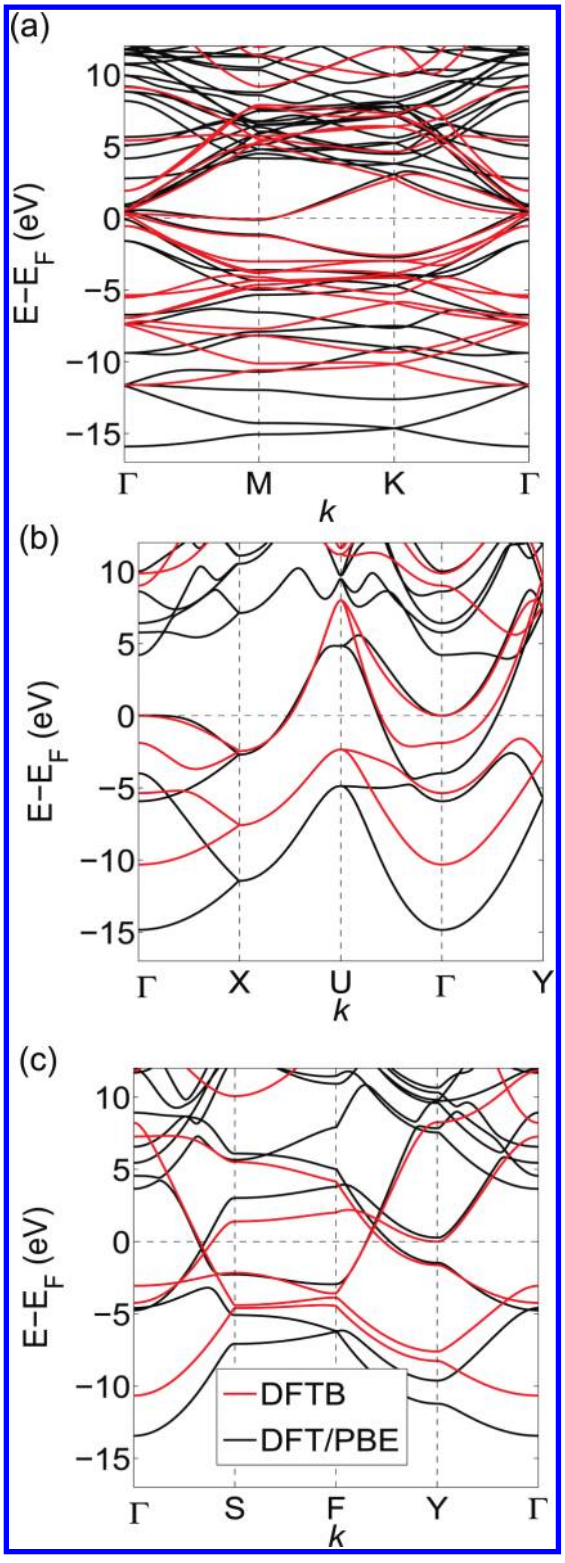

Figure 6. Comparison of band structures of three two-dimensional boron sheets obtained at the DFTB (red lines) and DFT/PBE (black lines) levels of approximation for the same geometry (taken from the DFT/PBE calculation): (a) α-sheet, (b) buckled triangular sheet, and (c) distorted hexagonal sheet. Valence bands qualitatively agree. Due to a relatively small basis set, DFTB shows fewer conduction bands than DFT/PBE. Close to the Fermi energy, DFTB accurately reproduces all bands.

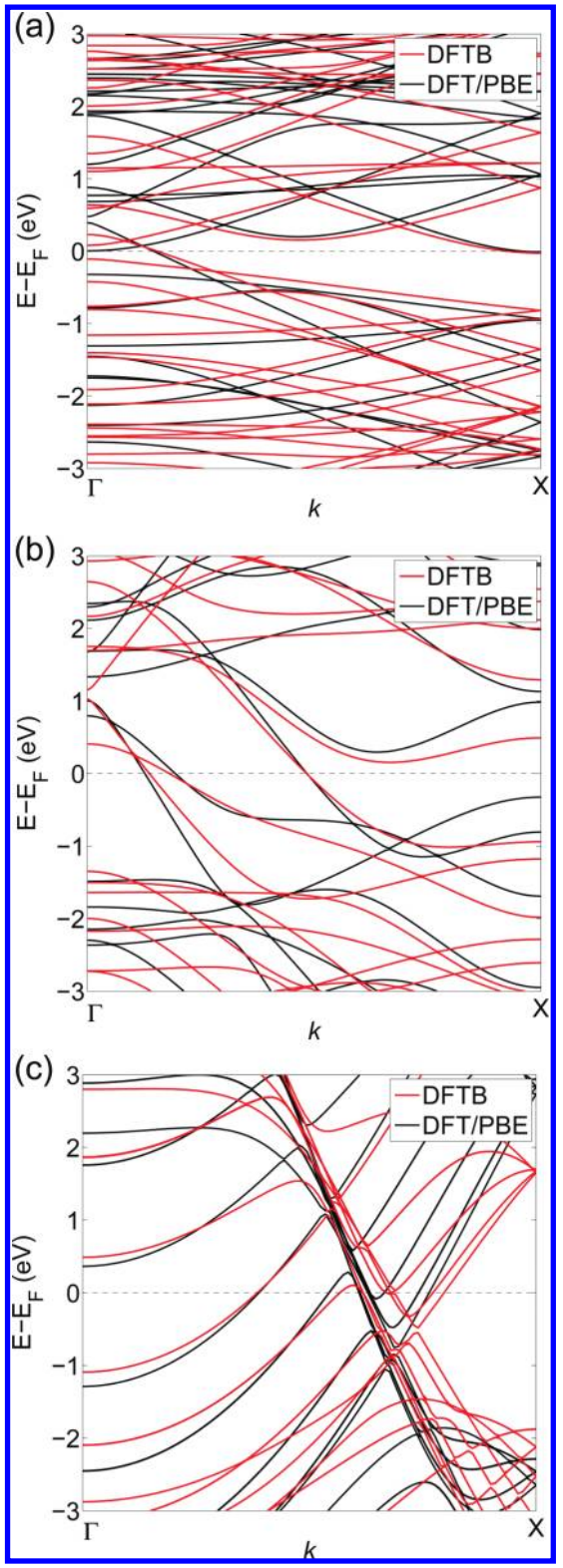

Figure 7. Comparison of band structures of three boron armchair nanotubes obtained at the DFTB (red lines) and DFT/PBE (black lines) levels of approximation for the same geometry (taken from the DFT/PBE calculation): (a) (4,0) α-BNT, (b) (0,12) BT-BNT, and (c) (4,4) DH-BNT.

DFTB overestimates E^{coh} on the average by ca. 1.0 eV/atom. Normalized to a single bond, we obtain an average overbinding of 0.366 eV = 8.4 kcal/mol. Such an overestimation is in agreement with the mentioned overbinding of the presented basis set by approximately 10 kcal/mol per bond.

dx.doi.org/10.1021/ct200722n | J. Chem. Theory Comput. 2012, 8, 1153–1163

Table 10. Cohesive (Atomization) Energies of Periodic Systems (in eV/atom) and DFTB Overbinding Per Bond (in kcal/mol)[a]

system	E^{coh} DFT/PBE	E^{coh} DFTB	overbinding per bond
α-rhombohedral	6.669	7.418	5.74
α-sheet	6.265	6.523	2.26
BT-sheet	6.178	8.038	14.25
DH-sheet	6.025	7.506	13.61
α-BNT (4,0)	6.175	6.517	2.99
BT-BNT (0,12)	5.912	6.78	6.14
DH-BNT (4,4)	5.924	7.428	13.82

[a]The spin polarization energy of isolated atoms was taken into account. No correction for zero point motion was performed.

4. SUMMARY

In this paper, we apply the SCC-DFTB method to boron and boranes. Our parametrization was tested for molecular and periodic systems in different properties like geometries, vibrational frequencies, atomization energies, and band structures. Although only the hypothetical molecule B_2H_4 was used as the needed fitting system, we achieved good transferability to other systems regardless of 2e3c bonds or periodic boundaries. For geometries and vibrations of molecules, we accomplish results near the level of B3LYP or PBE and do much better than AM1 and MNDO. While molecular atomization energies match the results of LDA calculations more than B3LYP or PBE, our minimal basis approach is effective to describe the band structures compared to PBE. This is also reflected in the results for the ionization of the dianion *closo* clusters, although DFTB predicts even $B_{12}H_{12}^{2-}$ to be unstable on its own. Therefore, our work presented here is a first step to enlarge the application possibilities of SCC-DFTB by including boron in the list of parametrized atoms.

AUTHOR INFORMATION

Corresponding Author

*E-mail: thomas.niehaus@physik.uni-regensburg.de.

Notes

The authors declare no competing financial interest.

ACKNOWLEDGMENTS

B.G.-S. and T.A.N. thank the University of Bremen (ZF 01/120/06) for financial support. V.B. and J.K. acknowledge financial support from the DFG (project KU 2347/2-1). We also acknowledge the Center for Information Services and High Performance Computing (ZIH) at the Dresden University of Technology for computational resources. G.C. is supported by World Class University program funded by the Ministry of Education, Science and Technology through the National Research Foundation of Korea (R31-10100).

REFERENCES

(1) Smith, H. W.; Lipscomb, W. N. *J. Chem. Phys.* **1965**, *43*, 1060.
(2) Nordman, C. E.; Lipscomb, W. N. *J. Chem. Phys.* **1953**, *21*, 1856.
(3) Dulmage, W. J.; Lipscomb, W. N. *Acta Crystallogr.* **1952**, *5*, 260.
(4) Longuet-Higgins, H. C.; Bell, R. P. *J. Chem. Soc.* **1943**, 250.
(5) Lipscomb, W. N. *Boron Hydrides*; W. A. Benjamin Inc.: New York, 1963.
(6) Wade, K. J. *J. Chem. Soc., Chem. Comm.* **1971**, 792.
(7) Wade, K. J. *Adv. Inorg. Radiochem.* **1971**, *18*, 1.
(8) Williams, R. E. *Chem. Rev.* **1992**, *92*, 177.
(9) Boustani, I. *Surf. Sci.* **1997**, *370*, 355.
(10) Boustani, I.; Quandt, A. *Europhys. Lett.* **1997**, *39*, 527.
(11) Zhai, H.-J.; Kiran, B.; Li, J.; Wang, L.-S. *Nat. Mater.* **2003**, *2*, 827.
(12) Kiran, B.; Bulusu, S.; Zhai, H.-J.; Yoo, S.; Zeng, X. C.; Wang, L.-S. *Proc. Natl. Acad. Sci. U.S.A.* **2005**, *102*, 961.
(13) Oger, E.; Crawford, N. R. M.; Kelting, R.; Weis, P.; Kappes, M. M.; Ahlrichs, R. *Angew. Chem., Int. Ed.* **2007**, *46*, 8503.
(14) Boustani, I. *J. Solid State Chem.* **1997**, *133*, 182.
(15) Szwacki, N. G.; Sadrzadeh, A.; Yakobson, B. I. *Phys. Rev. Lett.* **2007**, *98*, 166804.
(16) Boustani, I.; Quandt, A.; Hernadez, E.; Rubio, A. *J. Chem. Phys.* **1999**, *110*, 3176.
(17) Kunstmann, J.; Quandt, A. *Phys. Rev. B* **2006**, *74*, 035413−1.
(18) Lau, K. C.; Pati, R.; Pandey, R.; Pineda, A. C. *Chem. Phys. Lett.* **2006**, *418*, 549.
(19) Tang, H.; Ismail-Beigi, S. *Phys. Rev. Lett.* **2007**, *99*, 115501−1.
(20) Singh, A. K.; Sadrzadeh, A.; Yakobson, B. I. *Nano Lett.* **2008**, *8*, 1314.
(21) Yang, X.; Ding, Y.; Ni, J. *Phys. Rev. B* **2008**, *77*, 041402(R)−1.
(22) Ciuparu, D.; Klie, R. F.; Zhu, Y.; Pfefferle, L. *J. Phys. Chem. B* **2004**, *108*, 3967.
(23) Liu, F.; Shen, C.; Su, Z.; Ding, X.; Deng, S.; Chen, J.; Xu, N.; Gao, H. *J. Mater. Chem.* **2010**, *20*, 2197.
(24) Liu, J.; Iqbal, Z. *MRS Online Proc. Lib.* **2011**, *1307*, mrsf10-1307−cc05-21.
(25) Bezugly, V.; Kunstmann, J.; Grundkötter-Stock, B.; Frauenheim, T.; Niehaus, T.; Cuniberti, G. *ACS Nano* **2011**, *5*, 4997.
(26) Will, G.; Kiefer, B. *ZAAC* **2001**, *627*, 2100−2104.
(27) Lee, S.; Bylander, D. M.; Kleinman, L. *Phys. Rev. B* **1990**, *42*, 1316−1320.
(28) Slack, G. A.; Hejna, C. I.; Garbauskas, M. F.; Kasper, J. S. *J. Solid State Chem.* **1988**, *76*, 52.
(29) Vlasse, M.; Naslain, R.; Kasper, J. S.; Ploog, K. *J. Solid State Chem.* **1979**, *28*, 289.
(30) Wentorf, R. H. *Science* **1965**, *147*, 49.
(31) Zarechnaya, E. Y.; Dubrovinsky, L.; Dubrovinskaia, N.; Miyajima, N.; Filinchuk, Y.; Chernyshov, D.; Dmitriev, V. *Sci. Technol. Adv. Mater.* **2008**, *9*, 44209.
(32) Oganov, A. R.; Chen, J.; Gatti, C.; Ma, Y.; Ma, Y.; Glass, C. W.; Liu, Z.; Yu, T.; Kurakevych, O. O.; Solozhenko, V. L. *Nature* **2009**, *457*, 863.
(33) Porezag, D.; Frauenheim, T.; Köhler, T.; Seifert, G.; Kaschner, R. *Phys. Rev. B* **1995**, *51*, 12947.
(34) Seifert, G.; Porezag, D.; Frauenheim, T. *Int. J. Quantum Chem.* **1996**, *58*, 185.
(35) Elstner, M.; Porezag, D.; Jungnickel, G.; Elsner, J.; Haugk, M.; Frauenheim, T.; Suhai, S.; Seifert, G. *Phys. Rev. B* **1998**, *58*, 7260.
(36) Frauenheim, Th.; Seifert, G.; Elstner, M.; Niehaus, T. A.; Köhler, Ch.; Amkreutz, M.; Sternberg, M.; Hajnal, Z.; Di Carlo, A.; Suhai, S. *J. Phys. Condens. Mater.* **2002**, *14*, 3015.
(37) Seifert, G. *J. Phys. Chem. A* **2007**, *111*, 5609.
(38) Niehaus, T.; Elstner, M.; Frauenheim, T.; Suhai, S. *THEOCHEM* **2001**, *541*, 185.
(39) http://www.dftb.org/parameters/download/mio/mio_0_1/ (accessed Feb. 2012).
(40) Frisch, M. J.; Trucks, G. W.; Schlegel, H. B.; Scuseria, G. E.; Robb, M. A.; Cheeseman, J. R.; Montgomery, J. A., Jr.; Vreven, T.; Kudin, K. N.; Burant, J. C.; Millam, J. M.; Iyengar, S. S.; Tomasi, J.; Barone, V.; Mennucci, B.; Cossi, M.; Scalmani, G.; Rega, N.; Petersson, G. A.; Nakatsuji, H.; Hada, M.; Ehara, M.; Toyota, K.; Fukuda, R.; Hasegawa, J.; Ishida, M.; Nakajima, T.; Honda, Y.; Kitao, O.; Nakai, H.; Klene, M.; Li, X.; Knox, J. E.; Hratchian, H. P.; Cross, J. B.; Adamo, C.; Jaramillo, J.; Gomperts, R.; Stratmann, R. E.; Yazyev, O.; Austin, A. J.; Cammi, R.; Pomelli, C.; Ochterski, J. W.; Ayala, P. Y.; Morokuma, K.; Voth, G. A.; Salvador, P.; Dannenberg, J. J.; Zakrzewski, V. G.; Dapprich, S.; Daniels, A. D.; Strain, M. C.; Farkas, O.; Malick, D. K.; Rabuck, A. D.; Raghavachari, K.; Foresman, J. B.; Ortiz, J. V.; Cui, Q.; Baboul, A. G.; Clifford, S.; Cioslowski, J.; Stefanov, B. B.; Liu, G.; Liashenko, A.; Piskorz, P.; Komaromi, I.; Martin, R. L.; Fox, D. J.; Keith, T.; Al-Laham, M. A.; Peng, C. Y.; Nanayakkara, A.; Challacombe, M.; Gill, P. M. W.; Johnson, B.; Chen,

W.; Wong, M. W.; Gonzalez, C.; Pople, J. A. *Gaussian 03*, revision A.1; Gaussian, Inc.: Pittsburgh PA, 2003.
(41) Gaus, M.; Chou, C.-P.; Witek, H.; Elstner, M. *J. Phys. Chem. A* **2009**, *113*, 11866.
(42) Becke, A. D. *J. Chem. Phys.* **1993**, *98*, 5648−5652.
(43) Stephens, P. J.; Devlin, F. J.; Chabalowski, C. F.; Frisch, M. J. *J. Phys. Chem.* **1994**, *98*, 11623−11627.
(44) Perdew, J. P.; Burke, K.; Ernzerhof, M. *Phys. Rev. Lett.* **1996**, *77*, 3865−3868.
(45) Dewar, M. J. S.; Zoebisch, E. G.; Healy, E. F.; Stewart, J. J. P. *J. Am. Chem. Soc.* **1985**, *107*, 3902.
(46) Dewar, M. J. S.; Thiel, W. *Am. Chem. Soc.* **1977**, *99*, 4899.
(47) Frenzel, J.; Oliveira, A. F.; Jardillier, N.; Heine, T.; Seifert, G. *Semi-relativistic, self-consistent charge Slater-Koster tables for density-functional based tight-binding (DFTB) for materials science simulations.*; TU-Dresden: Dresden, Germany, 2004.
(48) http://www.dftb.org/parameters/download/matsci/matsci_0_3/ (accessed Feb. 2012).
(49) McKee, M. L.; Wang, Z.-X.; von Ragué Schleyer, P. *J. Am. Chem. Soc.* **2000**, *122*, 4781.
(50) Köhler, C.; Seifert, G.; Frauenheim, T. *Chem. Phys.* **2005**, 309.
(51) Kresse, G.; Joubert, D. *Phys. Rev. B* **1999**, *59*, 1758−1775.
(52) Kresse, G.; Furthmüller, J. *Phys. Rev. B* **1996**, *54*, 11169−11186.
(53) Paier, J.; Marsman, M.; Kresse, G. *J. Chem. Phys.* **2007**, *127*, 024103−1−0.
(54) Horn, F. H.; Taft, E. A.; Oliver, D. W. In *Boron*; Gaule, O. K.; Plenum Press: New York, 1965; Vol. 2, p 231.
(55) Golikova, O. A.; Solov'ev, N. E.; Ugai, Ya.A.; Feigel'man, V. A. *Fiz. Tekh. Poluprovodn.* **1979**, *13*, 825; *Sov. Phys. Semicond. (English Transl.)* **1979**, *13*, 486.
(56) Werheit, H.; Kuhlmann, U.; Solov'ev, N. E.; Tsiskarishvili, G. P.; Tsagareishvili, G. In *Boron-Rich Solids, Proc. 10th Int. Symp. Boron, Borides and Rel. Compounds*, Albuquerque, NM, 1990 (AIP Conf. Proc. 231), Emin, D., Aselage, T. L., Switendick, A. C., Morosin, B., Beckel, C. L., Eds.; American Institute of Physics: New York, 1991, p 350.